American Mineralogist, Volume 86, pages 681–689, 2001

Rare-earth elements in synthetic zircon: Part 2. A single-crystal X-ray study of xenotime substitution

ROBERT J. FINCH,[1,*] JOHN M. HANCHAR,[1,†] PAUL W. O. HOSKIN,[2,‡] AND PETER C. BURNS[3]

[1]Argonne National Laboratory, 9700 South Cass Avenue, Argonne, Illinios 60439, U.S.A.
[2]Research School of Earth Sciences, Institute of Advanced Studies, The Australian National University, Canberra ACT 0200, Australia
[3]Department of Civil Engineering and Geological Sciences, University of Notre Dame, Notre Dame, Indiana 46556-0767, U.S.A.

ABSTRACT

Zircon crystals synthesized in a Li-Mo oxide melt and doped with trivalent lanthanides and Y (REE), both with and without P, were examined by single-crystal X-ray diffraction (XRD). REE are incorporated into the Zr site in the zircon structure, and some Zr appears to be displaced to the Si site. Crystals doped with middle REE (MREE, Sm to Dy) and Y, plus P follow the xenotime substitution ($REE^{3+} + P^{5+} = Zr^{4+} + Si^{4+}$) rather closely, whereas crystals doped with heavy REE (HREE, Er to Lu) deviate from the xenotime substitution, having REE:P atomic ratios significantly greater than one. Xenotime substitution requires that P^{5+} replace Si^{4+}, but this substitution becomes limited by strain at the Si site in HREE-doped crystals. As Si sites become saturated with P^{5+}, additional charge balance in synthetic zircon crystals may be provided by Mo^{6+} and Li^{+} from the flux entering interstitial sites, accounting for an additional 0.3 to 0.6 at% HREE beyond that balanced by P^{5+} ions. Heavy REE are more compatible in the zircon structure than are LREE and MREE, and HREE substitution is ultimately limited by the inability of the zircon structure to further accommodate charge-compensating elements. Thus the limit on REE concentrations in zircon is not a simple function of REE^{3+} ionic radii but depends in a complex way on structural strain at Zr and Si sites, which act together to limit REE and P incorporation. The mechanisms that limit the coupled xenotime substitution change from LREE to HREE. This change means that REE fractionation in zircon may vary according to the availability of charge-compensating elements. REE partition coefficients between zircon and melt must also depend in part on the availability of charge-compensating elements and their compatibility in the zircon structure.

INTRODUCTION

Zircon is a ubiquitous accessory mineral in nature. The ability of zircon to retain chemical and isotopic information has led to its use in a wide range of geochemical investigations. Isotopic data gleaned from zircon can provide fundamental information about the evolution of the crust and differentiation of the mantle (Hanchar et al. 1994; Buick et al. 1995; Bowring 1995; Vervoot et al. 1996). U-Pb dating of zircon has long been used to unravel the timing of tectonic events and related processes, including orogenic episodes (Solar et al. 1998) and regional metamorphism (Gibson and Ireland 1995), even to constrain the duration of the Permian mass extinction (Bowring et al. 1998). The use of zircon as a dating tool is so well established that zircon ages have been used to support isotopic ages determined by other methods (Stein et al. 1998). The widespread use of zircon in geochronology reflects the exceptional durability of zircon under diverse geochemical conditions. For example, detrital zircons have been used to date processes such as river-basin development and provenance (Riggs et al. 1996) and sedimentation rates (Altermann and Nelson 1998).

In addition to its use as a geochronometer, zircon is an important geochemical indicator. For example, zircon crystals may preserve oxygen isotopic information through metasomatic events that disrupt oxygen isotopic ratios in other minerals (King et al. 1998; Taylor and Huston 1998). The extraordinary chemical durability of zircon is a critical factor in it being proposed as a candidate waste form for the geologic disposal of weapons-grade Pu (Ewing and Lutze 1997; Ewing 1999).

Although a minor constituent of most rocks in which they occur, accessory minerals such as zircon, monazite, xenotime, and apatite commonly account for most trace elements in felsic igneous and aluminous metamorphic rocks (Bea 1996a, 1996b). The extent to which an element becomes incorporated into a mineral that crystallizes from a liquid is expressed as a partition coefficient, $D = [M]_{mineral}/[M]_{liquid}$. Often, the only remnants of ancient liquids are the minerals left behind, and partition coefficients may provide the only information available about the composition of the parent liquid. Thus we hope to better

* E-mail: finch@cmt.anl.gov
† Present address: Department of Earth and Environmental Sciences, The George Washington University, Washington, D.C. 20006, U.S.A. Email: jhanch@gwu.edu
† Present address: Department of Civil Engineering adn Geological Sciences, 156 Fitzpatrick Hall, University of Notre Dame, Notre Dame, IN 46556, U.S.A. E-mail: phoskin@nd.edu

understand a diverse array of geochemical processes, including magma crystallization, metasomatism, metamorphism, even planetary differentiation, through a detailed understanding of mineral-melt partition coefficients (Ryerson and Hess 1978; Watson 1980; Blundy and Wood 1994).

The geochronological and geochemical importance of zircon requires that we understand processes that control trace-element distributions between zircon crystals and fluids (Watson et al. 1997; Cherniak et al. 1997; Lee et al. 1997). Indeed, there is evidence that metasomatism can disrupt Nd-Sm systematics in zircon (Odling 1995; Vervoot et al. 1996). Structural damage to zircon, caused primarily by alpha decay of radioactive elements in the zircon structure, may also affect zircon chemistry and isotopic systematics after formation (McLaren et al. 1991). Radiation-damaged zircon crystals may exhibit enhanced diffusion (Watson and Cherniak 1997; Lee et al. 1997; Meldrum et al. 1998), reduced structural integrity (Chakoumakos et al. 1987; Murakami et al. 1991), and enthalpy changes that could increase solubilities (Ellsworth et al. 1994).

Zircon commonly contains trace amounts (or more) of P, Y, Hf, U, Th, and lanthanides (Speer 1982). Both natural and synthetic zircon crystals are commonly enriched in Y and heavy rare-earth elements (HREE) relative to light and middle rare earths (LREE and MREE) (Nagasawa 1970; Watson 1980; Speer 1982; Gromet and Silver 1983; Fujimaki 1986; Heaman et al. 1990; Hinton and Upton 1991; Hanchar et al. 2001). Subtle differences in ionic radii of REE and different redox sensitivities among certain REE (e.g., Ce and Eu) can produce pronounced chemical differences among REE-bearing minerals, including zircon (Rollinson 1993).

Zircon is isostructural with xenotime (YPO_4), and REE-bearing zircon crystals commonly contain P (Speer 1982; Hinton and Upton 1991; Belousova et al. 1998). Owing to close crystal-chemical similarities between Y^{3+} and heavy REE^{3+}, the replacement of Zr^{4+} by REE^{3+} in zircon is commonly explained by the coupled xenotime-type substitution, in which P^{5+} replaces Si^{4+}, maintaining charge balance according to the substitution $REE^{3+} + P^{5+} = Zr^{4+} + Si^{4+}$ (Speer 1982). Implicit in the xenotime substitution is the assumption that P^{5+} in zircon replaces Si^{4+} in the tetrahedral site and REE replace Zr^{4+} in the 8-coordinated Zr site; thus the ideal formula for xenotime-substituted zircon is $REE_xZr_{1-x}P_xSi_{1-x}O_4$, in which x indicates the mole fraction of xenotime. If xenotime substitution is the only mechanism by which charge balance is maintained in REE-substituted zircon, the ratio REE:P must be unity; however, atomic ratios of REE:P measured in natural and synthetic zircon crystals commonly deviate significantly from one (Speer 1982; Hinton and Upton 1991; Maas et al. 1992; Hanchar et al. 2001), indicating a more-complex charge-balance mechanism (or multiple mechanisms). Natural zircon crystals may exhibit charge-preserving substitutions besides, or in addition to, xenotime substitution, including exchange of OH^- groups for O^{2-} ions and coupled substitution at the Zr site (Speer 1982 and references therein).

To elucidate the structural roles of P and REE in zircon due to the xenotime substitution, and to test the hypothesis that incorporation of REE^{3+} into zircon is solely a function of ionic radius (Hinton and Upton 1991; Blundy and Wood 1994), we examined several REE- and P-doped synthetic zircon crystals by single-crystal XRD. To reduce ambiguities that might be caused by simultaneous substitutions of different REE, each synthetic zircon crystal contains only one REE. Zircon crystals were synthesized in an anhydrous Li-Mo-oxide flux, to which REE_2O_3 and P_2O_5 were added in equal molar proportions (Hanchar et al. 2001 provide details of the synthesis). This synthesis method produced zircon crystals that displayed slight nonstoichiometry, with the exceptions of pure $ZrSiO_4$, and Gd- and Tb-doped crystals, which are stoichiometric within analytical uncertainty (2σ). All other synthetic zircon crystals have slight excesses of Zr-site cations (Zr and REE) that correlate negatively with slight deficits in Si-site cations (Si and P). This non-stoichiometry is evident throughout entire crystals, regardless of chemical zoning, and is not correlated with REE content (Hanchar et al. 2001). Therefore, an additional goal of this study was to discern structural details caused by the observed nonstoichiometry in these crystals. We limited XRD examinations to selected crystals doped with Sm and heavier REE. Crystals examined by XRD are indicated as filled symbols in Figure 1, which illustrates the variation in P with REE for all synthetic zircon crystals reported by Hanchar et al. (2001).

EXPERIMENTAL METHODS

XRD data collection

Single crystals of synthetic zircon were examined with a Bruker PLATFORM 3-circle goniometer equipped with a 1K SMART charge-coupled device (CCD) detector with a crystal-to-detector distance of 5 cm. Data were collected by using monochromatic Mo$K\alpha$ X-rays (λ = 0.71073 Å), with frame widths of 0.3° in ω, and were acquired for 10 seconds per frame (Burns 1998 discusses the application of CCD detectors to structure analyses by XRD). Three-dimensional data were collected

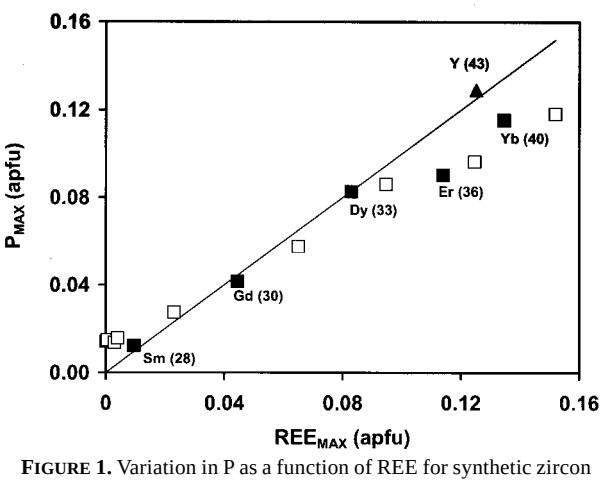

FIGURE 1. Variation in P as a function of REE for synthetic zircon crystals (data are from Hanchar et al. 2001). Filled symbols indicate crystals examined by XRD: squares indicate crystals doped with lanthanides; the triangle indicates the [Y+P]-doped crystal (crystal 43). The solid line illustrates the trend predicted for xenotime substitution ($REE^{3+} + P^{5+} = Zr^{4+} + Si^{4+}$). If the only mechanism for maintaining charge balance is the xenotime substitution, data plotting above the line indicate excess positive charge and those below the line indicates excess negative charge.

TABLE 1. Crystal data and structure-refinement details for synthetic zircon crystals

	$ZrSiO_4$ (38)*	Dy (15)	Dy (12)	Sm+P (28)	Gd+P (30)	Dy+P (33)	Er+P (36)	Yb+P (40)	Y+P (43)
Unit cell parameters (Å)†	a = 6.6102(8) c = 5.986(1)	a = 6.6139(8) c = 5.985(1)	a = 6.6175(8) c = 5.989(1)	a = 6.6119(8) c = 5.983(1)	a = 6.6213(7) c = 5.9879(9)	a = 6.626(1) c = 5.986(1)	a = 6.6355(8) c = 5.989(1)	a = 6.6265(8) c = 5.979(1)	a = 6.6329(8) c = 5.986(1)
V (Å^3)†	261.57(6)	261.82(6)	262.26(6)	261.54(6)	262.52(6)	262.79(10)	263.69(6)	262.53(6)	263.37(6)
density$_{calc}$ (g/cm^3)	4.655	4.670	4.711	4.655	4.788	4.795	4.905	4.886	4.656
Abs. coeff. (mm^{-1})	4.382	4.539	4.769	4.383	6.281	6.574	7.716	8.135	6.688
F(000)	344	345	348	344	353	354	363	359	347
2θ range for data	9.18–56.50°	9.18–56.48°	9.18–56.44°	9.18–56.50°	9.18–56.42°	9.18–56.40°	9.18–56.54°	9.18–56.62°	9.18–56.34°
Index ranges	$-8\le h\le 7$ $-8\le k\le 8$ $-7\le l\le 4$	$-8\le h\le 8$ $-8\le k\le 7$ $-7\le l\le 4$	$-6\le h\le 8$ $-7\le k\le 8$ $-7\le l\le 7$	$-8\le h\le 7$ $-8\le k\le 8$ $-7\le l\le 4$	$-5\le h\le 8$ $-8\le k\le 8$ $-7\le l\le 7$	$-8\le h\le 8$ $-8\le k\le 8$ $-7\le l\le 5$	$-8\le h\le 7$ $-8\le k\le 8$ $-7\le l\le 6$	$-7\le h\le 8$ $-7\le k\le 8$ $-6\le l\le 7$	$-8\le h\le 8$ $-8\le k\le 8$ $-6\le l\le 7$
Total I	641	667	601	636	656	715	632	748	676
Unique I	96	96	97	97	97	97	98	98	97
$R_{(int)}$ (%)	3.68	2.54	2.49	2.75	3.00	2.57	2.10	2.35	2.30
GoF‡ on F^2	1.257	1.405	1.240	1.233	1.157	1.354	1.238	1.346	1.224
R indices§ [all data] (%)	R_1 = 4.22 wR_2 = 10.65	R_1 = 1.79 wR_2 = 3.55	R_1 = 1.63 wR_2 = 3.64	R_1 = 1.63 wR_2 = 3.83	R_1 = 1.42 wR_2 = 2.78	R_1 = 1.20 wR_2 = 3.08	R_1 = 1.05 wR_2 = 2.83	R_1 = 0. 99, wR_2 = 2.51	R_1 = 1.51 wR_2 = 3.50
Extinction coeff. †	2.1(4)	0.262(14)	0.151(13)	0.124(8)	0.013(2)	0.007(2)	0.0062(13)	0.0122(14)	0.014(2)
Largest diff. peak & hole (e/Å^3)	1.302 & –2.688	0.443 & –0.855	0.558 & –0.840	0.522 & –0.524	0.440 & –0.383	0.539 & –0.290	0.378 & –0.305	0.478 & –0.299	0.392 & –0.974

* The pure $ZrSiO_4$ crystal was "shocked" by immersing it in liquid N_2.
† Values in parentheses are 1σ estimated standard deviation in the last decimal place.
‡ Goodness of Fit (GoF) = $\{\Sigma [w(F_o^2 - F_c^2)^2]/ (n - p)\}$, where n is the number of data (F_o) and p is the number of refined parameters.
§ Agreement factors: $R_1 = \Sigma||F_o| - |F_c||/\Sigma|F_o|$; $wR_2 = \{\Sigma[w(F_o^2 - F_c^2)^2]/\Sigma[w(F_o^2)^2]\}$; $w = [\sigma^2 F_o^2 + (0.0075\ P)^2 + 0.39\ P]^{-1}$ where $P = [\max.(F_o^2,0) + 2F_c^2]/3$.

from more than one hemisphere for each crystal. Data were analyzed to locate peaks for determining unit-cell dimensions (Table 1), which were calculated from approximately 740 strong reflections by least-squares refinement. Quantitative intensity data were collected over the range $3° < 2\theta < 56.6°$ during approximately 6 hours for each crystal; intensities from equivalent reflections displayed no significant decay during any data-collecting session. Three-dimensional data were integrated and corrected for Lorentz, polarization, and background effects with the Bruker program SAINT and reduced to structure factors. An empirical absorption correction was applied to data from each crystal by using the program SADABS (G. Sheldrick, unpublished computer program), based on ~550 intense reflections and by modeling crystals as ellipsoids. Approximately 630 reflections consistent with I centering were collected for each crystal, of which 98 were unique and 96, 97, or 98 are considered "observed" ($|F| > 4\sigma_F$) (Table 1).

Structure refinements

Starting atomic positions for all structure refinements were from Hazen and Finger (1979). Zr and Si occupy special positions in space group $I4_1/amd$; only y/b and z/c coordinates of the O site are refineable. All structure refinements converged smoothly and rapidly and were run until the largest shift/ESD (estimated standard deviation) was less than 0.0005. Data were refined by full-matrix least squares on F^2 with the program package SHELXL-93. We used ionic scattering factors for cations from the *International Tables for X-ray Crystallography* (Ibers and Hamilton 1974) and ionic scattering factors for O^{2-} from Azavant and Lichanot (1993). Anisotropic displacement parameters for all atoms were refined independently. To determine relative amounts of Zr and REE at the Zr site for those crystals in which Zr-site occupancies refined high [i.e., crystals 12 (Dy), 28 (Sm+P), 30 (Gd+P), 33 (Dy+P), 36 (Er+P), and 40 (Yb+P)], the Zr sites were split between Zr and REE, with the sum of site-occupancy factors (SOF) for the split site fixed [note that XRD cannot distinguish Zr (Z = 40) and Y(Z = 39), precluding refinement of the Zr-site SOF in crystal 43 (Y+P)]. Agreement factors (R_1 and wR_2) and the magnitudes of extinction parameters decrease for zircon crystals with increasing REE concentrations (Table 1), a result probably caused by decreasing crystal perfection due to increased strain in synthetic zircon crystals with increased REE and P concentrations (see Discussion section below).

Agreement factors indicate excellent model agreement, except for the $ZrSiO_4$ crystal, which suffers severe effects of secondary extinction (Table 1). That crystal was "shocked" by immersing it in liquid N_2, which reduced the extinction coefficient and agreement index by approximately one half. Final maximum electron-density peaks and holes in difference-Fourier maps for each refinement are listed in Table 1. Data from crystals 30 (Gd+P), 33 (Dy+P), 36 (Er+P), 40 (Yb+P), and 43 (Y+P) display minor residual electron peaks (0.4 to 0.5 e/Å^3) midway between the Si and O sites, whereas most residual electron density for crystals 12 (Dy) and 15 (Dy) is associated with the Zr site (Table 1). The final difference-Fourier map for $ZrSiO_4$ indicates significant residual electron density, which we attribute to problems caused by secondary-extinction effects.

RESULTS

Site occupancies

Electron densities measured at the Zr site increase with increased REE concentrations (Fig. 2a). Figure 2a illustrates the variation in the number of REE atoms per formula unit (apfu) as a function of the REE apfu calculated from electron microprobe analyses (EMPA) (Hanchar et al. 2001). The solid line in Figure 2a illustrates the trend predicted for Zr-site occupancy factors if they were equal to those calculated from EMPA data. Hanchar et al. (2001) demonstrated that REE-doped zircon crystals are compositionally zoned, with REE concentrations decreasing from the centers of crystals to the rims. Because XRD data are collected from whole crystals, REE apfu determined from refined site-occupancy factors (SOFs) must be less than REE apfu calculated from EMPA data, which correspond in this case to maximum REE concentrations measured at the central regions of synthetic zircon crystals. Figure 2a illustrates that average REE compositions for whole crystals are approximately 60% of maximum REE concentrations.

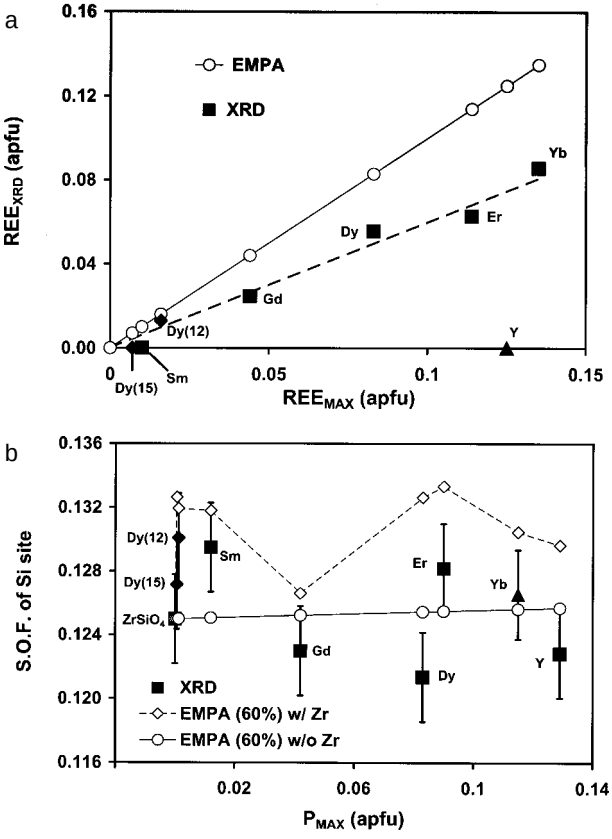

FIGURE 2. Observed site occupancy factors (SOF) (**a**) at the Zr site and (**b**) at the Si site, determined by single-crystal XRD. Solid line in (**a**) shows calculated REE apfu from maximum EMPA concentrations (Hanchar et al. 2001); dashed line shows calculated REE apfu for 60% of reported EMPA values. Solid line in (**b**) illustrates SOFs calculated by assuming only Si and P in the Si site; dashed line shows same calculation assuming all Zr in excess of Zr + REE = 1 occurs at Si site (both calculations are based on 60% of reported EMPA concentrations). Diamonds represent Dy-doped crystals without added P (crystals 15 and 12); the triangle represents the [Y+P]-doped crystals (crystal 43). Note that Y [Z = 39] cannot be distinguished from Zr [Z= 40] by XRD, so that crystal 43 [Y+P] plots at REE = 0 in (**a**).

Most synthetic zircon crystals are not stoichiometric but have (Zr+REE) apfu slightly exceeding one. However, excess (Zr+REE) is not correlated with REE content (Hanchar et al. 2001); rather, the sum (Zr + REE) is negatively correlated with the sum (Si + P), such that the sum of all cations equals 2 apfu. Nearly all excess (Zr+REE) is accounted for by excess Zr alone. Substitution of $^{IV}Zr^{4+}$ (ionic radius 0.46 Å) at the Si site will be manifested as longer bond distances and higher electron densities than for stoichiometric crystals. Measured electron densities at the Si site show little significant variation (within 2s) with P and REE concentrations, and most do not deviate significantly from values expected for stoichiometric crystals (solid line in Fig. 2b); however, with the exceptions of crystals 33 [Dy+P] and 43 [Y+P], the *trend* of variations in measured Si-site-occupancy factors approximately follows that of Si-site-occupancy factors calculated by assuming all Zr in excess of Zr + REE = 1 occurs in Si sites (dashed line in Fig. 2b).

Structural strain

Unit-cell volumes of synthetic zircon crystals (261.5–263.4 Å^3, Table 1) are within the range of, or just slightly greater than unit-cell volumes of natural zircon crystals reported by Speer (1982: 260.8 to 263.32 Å^3). With increasing REE and P contents, synthetic zircon crystals exhibit a general increase in the *a* cell dimension; however, rather than increasing as a simple function of REE content, the maximum *a* cell dimension is exhibited by the Er-doped crystal. The *a* cell dimension decreases slightly from this maximum for crystals doped with Y and Yb, even though they have higher REE contents (Table 1). The *c* cell dimension shows a rather weak correlation with REE, remaining approximately constant for crystals with REE concentrations up to that of the Y-doped crystal. The Yb-doped crystal, with the highest REE content among the crystals examined by XRD, has the smallest *c* cell dimension (Table 1). Both *a* and *c* cell dimensions of Er-, Y-, and Yb-doped crystals decrease sharply as REE and P contents increase. Changes in unit-cell volume correlate most strongly with changes in the *a* cell dimension but correlate weakly with changes in the *c* cell dimension. Pure $ZrSiO_4$ and the Sm-doped zircon crystal exhibit the smallest unit-cell volumes; the Er-doped zircon crystal has the largest (Table 1).

Two distinct Zr-O bond distances define the Zr dodecahedron in the zircon structure. The short bond distance increases from a minimum of 2.130 Å in crystal 28 (Sm+P) and pure $ZrSiO_4$ to a maximum of 2.142 Å in crystal 36 (Er+P) (Table 2). The longer Zr-O bond distance increases from a minimum of 2.270 Å to a maximum of 2.278 Å in crystals 28 (Sm+P) and 36 (Er+P), respectively (Table 2). The two Zr-O bond distances reported by Hazen and Finger (1979) for a natural zircon crystal are 2.128 and 2.267 Å, slightly shorter than corresponding bond distances in the synthetic zircon crystals. Substitution of large REE^{3+} ions into the Zr site is expected to increase Zr-O bond distances, and substitution of P^{5+} at the Si

TABLE 2. Selected bond lengths (Å) and O-Si-O angles (°) in REE-doped synthetic zircon crystals*

Crystal	Zr-O	Zr-O'	<Zr-O>	$(d-d_o)/d_o$ (<Zr-O>)†	Si-O	$(d-d_o)/d_o$ (Si-O)†	∠O-Si-O	∠O-Si-O'
$ZrSiO_4$ (38)	2.130(4)	2.275(4)	2.2025	+0.11%	1.622(4)	–0.12%	97.4(3)	115.8(2)
Dy (15)	2.1309(12)	2.2719(13)	2.2014	+0.06%	1.6247(2)	+0.04%	97.15(9)	115.96(5)
Dy (12)	2.1318(12)	2.2740(13)	2.2029	+0.13%	1.6254(5)	+0.09%	97.20(9)	115.93(5)
Sm+P (28)	2.130(2)	2.270(2)	2.2000	—	1.624(2)	—	97.12(11)	115.98(6)
Gd+P (30)	2.1348(14)	2.2755(14)	2.2052	+0.23%	1.6231(14)	–0.06%	97.31(10)	115.87(6)
Dy+P (33)	2.140(2)	2.276(2)	2.2080	+0.36%	1.620(2)	–0.25%	97.34(11)	115.86(6)
Er+P (36)	2.142(2)	2.278(2)	2.2100	+0.45%	1.622(2)	–0.12%	97.46(11)	115.79(6)
Yb+P (40)	2.140(2)	2.275(2)	2.2075	+0.34%	1.618(2)	–0.37%	97.49(11)	115.77(6)
Y+P (43)	2.1414(12)	2.2775(12)	2.2095	+0.43%	1.6207(12)	–0.20%	97.47(9)	115.78(5)
natural‡	2.128	2.267	2.198		1.623		97.0	116.1

* Values in parentheses are 1σ estimated standard deviation in the last decimal place.
† Relative differences in bond lengths are calculated as the percentage difference between d (the observed bond length in the crystal analyzed) and d_o (the equivalent bond length in the [Sm+P]-doped crystal (crystal 28), which has the shortest Zr-O bond distances). For consistency, Si-O bond distances are compared with the Sm-doped crystal as well.
‡ Hazen and Finger (1979).

site may enhance this somewhat.

As noted above, site-occupancy factors for the Zr site indicate that REE concentrations averaged over entire crystals are approximately 60% of maximum compositions (Fig. 2a). Therefore, we estimated expected Zr-O bond distances by using 60% of maximum EMPA concentrations to calculate bond-valence sums to the Zr site in each synthetic zircon crystal. Average Zr-O bond distances measured by XRD are slightly shorter than those calculated from EMP anaylsis in all synthetic zircon crystals (Fig. 3a). Deviations from calculated (EMPA) average bond distances are within analytical uncertainty (2σ) for most crystals; however, Zr-O distances are significantly shorter than expected for crystals 40 (Y+P) and 43 (Yb+P).

The large difference between ionic radii of tetrahedrally coordinated P^{5+} and Si^{4+} ions (0.17 and 0.26 Å, respectively) makes the Si-O bond distance sensitive to relatively small substitution of P^{5+} at the Si site. Among synthetic zircon crystals that contain both REE and P, the Si-O bond distance varies from a minimum of 1.618 Å (Yb+P) to a maximum of 1.624 Å (Sm+P) (Table 2), values that bracket the Si-O bond distance of 1.623 Å reported by Hazen and Finger (1979). The longest Si-O bond distances are exhibited by the two Dy-doped crystals synthesized without adding P to the flux: 1.6247 Å and 1.6254 Å for crystals 15 and 12, respectively (Table 2). In the absence of other effects, substitution of P^{5+} into the Si site will shorten Si-O bond distances. Expected Si-O bond distances were calculated by assuming that 60% of maximum P concentrations by EMPA accurately reflect average concentrations of entire crystals (cf. Fig. 2a). Two cases were considered, that for which only Si and P occur at the Si site (solid line in Fig. 3b) and that for which all Zr in excess of Zr + REE = 1 also occurs at the Si site (dashed line in Fig. 3b). Measured (XRD) Si-O bond distances are slightly longer than expected if we assume that no Zr occurs at the Si site, although most are within the uncertainty (2σ) of calculated Si-O bond distances. Notable exceptions are crystals 36 (Er+P) and 43 (Y+P), for which measured (XRD) Si-O bond distances are significantly longer than expected if no Zr occurs at the Si site (Fig. 3b). The Si-O bond distance in crystal 43 shows excellent agreement with the Si-O bond distance calculated by assuming Zr occurs at the Si site.

The SiO_4 tetrahedron in zircon is distorted, being slightly elongated along *c* (Hazen and Finger 1979; Speer 1982). The two O-Si-O angles in $ZrSiO_4$, 97.4(3)° and 115.8(2)°, are similar to O-Si-O angles of 97.0 and 116.1° reported by Hazen and Finger (1979). As REE contents increase from the Sm-doped crystal to the Yb-doped crystal, the larger O-Si-O angle decreases slightly from 115.98 to 115.77° and the smaller O-Si-O angle increases from 97.12 to 97.49° (Table 2). Thus, distortion of the SiO_4 tetrahedron actually decreases with increased REE and P contents.

TABLE 3. Refined fractional coordinates and anisotropic displacement parameters* (Å² x 10³) for O atom in $ZrSiO_4$

	y	*z*	U_{11}	U_{22}	U_{33}	U_{23}	*U*(eq)
$ZrSiO_4$ (38)	0.0657(5)	0.1961(7)	10(2)	6(2)	3(2)	0(1)	6(1)
Dy (15)	0.0658(2)	0.1954(2)	12(1)	9(1)	8(1)	0(1)	10(1)
Dy (12)	0.0658(2)	0.1955(2)	11(1)	7(1)	7(1)	0(1)	9(1)
Sm+P (28)	0.0658(2)	0.1953(2)	9(1)	6(1)	6(1)	0(1)	7(1)
Gd+P (30)	0.0660(2)	0.1959(2)	8(1)	6(1)	5(1)	0(1)	6(1)
Dy+P (33)	0.0664(2)	0.1963(3)	8(1)	5(1)	5(1)	0(1)	6(1)
Er+P (36)	0.0663(2)	0.1964(2)	10(1)	7(1)	6(1)	0(1)	8(1)
Yb+P (40)	0.0664(2)	0.1965(2)	9(1)	6(1)	6(1)	0(1)	7(1)
Y+P (43)	0.0663(2)	0.1964(2)	8(1)	7(1)	6(1)	0(1)	7(1)

* The anisotropic displacement-parameter exponent takes the form: $-2\pi^2[h^2\mathbf{a}^{*2}U_{11} + \ldots + 2hk\,\mathbf{a}^*\mathbf{b}^*U_{12}]$; *U*(eq) is defined as one third of the trace of the orthogonalized U_{ij} tensor. Values of *x*, U_{13}, and U_{33} are zero.

TABLE 4. Ions that may substitute in synthetic zircon crystals

Si site	Ionic radius* (Å)	Zr site	Ionic radius* (Å)
$^{IV}P^{5+}$	0.17	$^{VIII}Zr^{4+}$	0.86
$^{IV}Si^{4+}$	0.26	$^{VIII}REE^{3+}$	1.16–0.977
$^{IV}Mo^{6+}$	0.41	$^{VII}Mo^{6+}$	0.73
$^{IV}Zr^{4+}$	0.59	$^{VI}Li^{+}$	0.76
$^{IV}Li^{+}$	0.59	$^{VII}Li^{+}$	0.92

* Ionic radii from Shannon (1976).

The only refineable atomic positional parameters in zircon are the fractional coordinates of the O site: *y*/*b* and *z*/*c* (Table 3). As REE contents increase in synthetic zircon crystals, the O site shifts parallel to {100}, approximately along <012> (Fig. 4). Values of the *y* coordinate range from 0.0657 in $ZrSiO_4$ to 0.0663 for crystals 36 (Er+P) and 40 (Yb+P), and the *z* coordinate ranges from 0.1953 (Sm+P) to 0.1965 (Yb+P). These values are similar to, though slightly greater than values of 0.0660 and 0.1951 reported by Hazen and Finger (1979). The total change in the O-site coordinates corresponds to a net shift of approximately 0.01 Å along <012> as REE and P contents in-

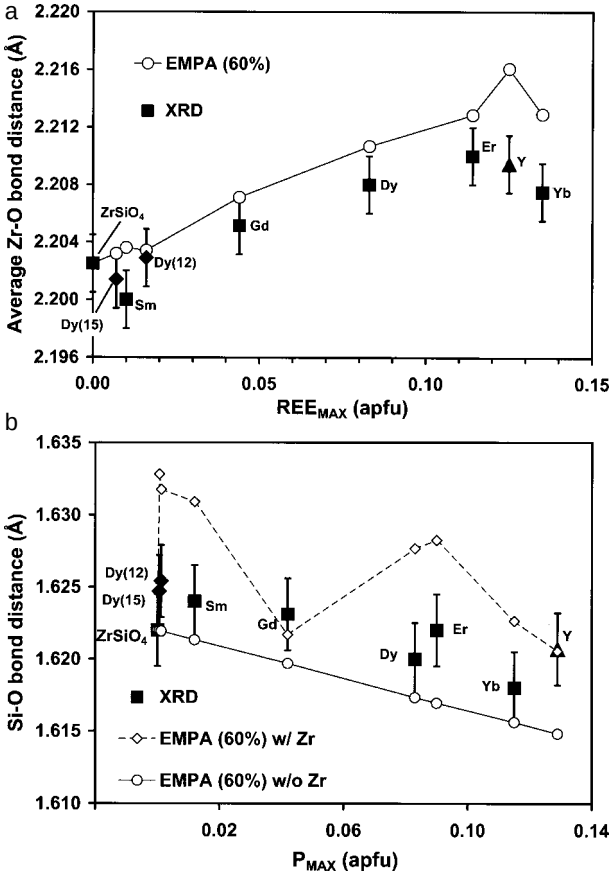

FIGURE 3. Observed bond distances for (**a**) average Zr-O and (**b**) Si-O determined by single-crystal XRD. Expected average Zr-O bond distances (open circles with solid line in **a**) were calculated by summing weighted bond-valence contributions to the Zr site from individual bonds before calculating averages (bond-valence parameters for REE and Zr from Brown 1981). Expected Si-O bond distances were calculated with ionic radii from Shannon (1976): solid line illustrates calculated Si-O distances assuming only Si and P at the Si site; dashed line shows same calculation but assuming all Zr in excess of Zr + REE = 1 occurs at Si site. Calculated bond distances are based on 60% of reported EMPA concentrations. Symbols as for Figure 2.

crease, with the O site moving away from the two neighboring Zr sites and toward (though not directly toward) the Si site.

DISCUSSION

If variations in REE concentrations of synthetic zircon crystals depended solely on variations in the ionic radii of REE^{3+} cations, we should expect to observe REE concentrations increase smoothly and steadily as REE^{3+} ionic radii decrease from La^{3+} to Lu^{3+} (Table 4). Hanchar et al. (2001) demonstrate that this is not true (cf., Fig. 3 in Hanchar et al.). Clearly, some additional factor or factors influence the incorporation of REE into synthetic zircon crystals. Figure 1 shows the variation in P as a function of REE for synthetic zircon crystals, as reported by Hanchar et al. (2001) from EMPA data. The solid line in Figure 1 shows the trend consistent with xenotime-type substitution (REE = P). Crystals doped with light and medium REE follow the expected trend rather well, although some "excess"

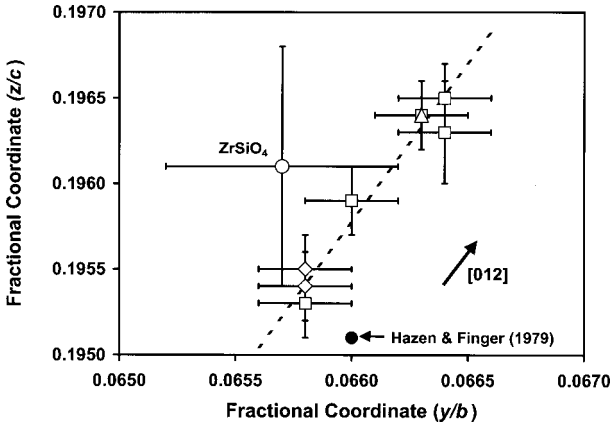

FIGURE 4. Variation in the fractional coordinates, z/c as a function of y/b for the O site in synthetic zircon. Dotted line shows least-squares fit to data for REE-doped crystals. Filled circle corresponds to values reported by Hazen and Finger (1979) for a natural zircon crystal. Vector indicates the [012] direction in zircon.

P is evident in LREE-doped crystals (which were not analyzed by XRD). Crystal 43 [Y+P] also falls very near the expected xenotime trend. Deviations from the xenotime trend are most significant for crystals doped with HREE (Er, Tm, Yb, Lu). Crystals with REE and P concentrations that deviate from the xenotime trend may be viewed either as containing excess REE or being deficient in P. The EMPA data indicate that, as REE concentrations increase, P concentrations in zircon crystals approach that of crystal 43 [Y+P] (Fig. 1). A possible explanation for this observation is that the Si site becomes saturated with P, possibly because the zircon structure can accommodate no further strain associated with substitution of the smaller P^{5+} cation at this site.

The EMPA data indicate slight non-stoichiometry among most REE-doped crystals (Hanchar et al. 2001). Non-stoichiometry in zircon crystals might be explained either by REE occupying interstitial sites in the zircon structure or REE displacing Zr from the Zr site, which might then enter interstitial sites. Both explanations are problematic, because the observed non-stoichiometry is not correlated with REE content (Hanchar et al. 2001). Also, as noted above, all significant excess electron density in difference Fourier maps for crystals examined by XRD is associated with cation sites, with no measurable electron density at interstitial sites. This finding indicates that cations do not occupy interstitial sites in detectable amounts, because, if all excess REE (or Zr) were interstitial, they should give rise to measurable excess electron density at interstitial sites.

More importantly, the slight excesses of Zr-site cations (Zr and REE) correlate with slight deficiencies in Si-site cations (Si and P), with the exceptions of Gd- and Tb-doped crystals (both of which are stoichiometric within 2σ). The observed non-stoichiometry is not limited to crystal cores, but is evident throughout entire crystals (Hanchar et al. 2001). Such a relationship suggests that Zr substitutes for Si at the Si site in synthetic crystals [the large differences in ionic radii between Si^{4+} (0.26 Å) and REE^{3+} (~1 Å) make it highly unlikely for REE^{3+} to occur in the Si site].

Our XRD results strongly suggest that REE occur only at the Zr site, consistent with the xenotime substitution, whereas conclusions about the Si site are more ambiguous. Within the uncertainty of our data, Si SOFs and Si-O bond distances cannot be used to argue either for or against Zr substitution at the Si site; however, because the trends of data in Figures 2b and 3b qualitatively follow those predicted by assuming minor Zr occurs at the Si site, we suspect that minor Zr has replaced Si in synthetic zircon crystals. This conclusion is also consistent with EMPA data, which show a nearly perfect negative correlation between Zr-site cations and Si-site cations (see Fig. 4 in Hanchar et al. 2001). We suggest, therefore, that excess Zr in the Si site best explains the observed non-stoichiometry in synthetic zircon crystals.

An important question is how charge balance is maintained in synthetic zircon crystals that contain REE in excess of P. There must be some mechanism besides P^{5+} substitution alone that helps accommodate apparent charge imbalances in HREE-doped crystals. Although O^{2-} vacancies might be invoked for charge balance, we believe this is highly unlikely given the problematic configuration of an SiO_3^{2-} group in the zircon structure. Furthermore, the calculated energy for O-vacancy migration in zircon, 1.16 to 1.38 eV (Williford et al. 1999), is less than that of O-vacancy formation: 1.7 eV, (Crocombette 1999). Substantial concentrations of static O-site vacancies are therefore unlikely to persist in the zircon structure.

Minor substitution of flux-derived Mo^{6+} for Si^{4+} or Zr^{4+} would provide some charge compensation in HREE-doped zircon crystals for which REE exceed P through the coupled substitutions $Mo^{6+} + 2REE^{3+} = Si^{4+} + 2Zr^{4+}$ and $Mo^{6+} + 2REE^{3+} = 3Zr^{4+}$, and Caruba et al. (1995) found that Mo^{6+} occupies Si sites in Mo-substituted synthetic zircon. The ionic radius of four-coordinated Mo^{6+} (0.41 Å) is compatible with minor substitution at the Si site, and the ionic radius of seven-coordinated Mo^{6+} (0.74 Å) suggests it may also occur at the (eight-coordinated) Zr site in minor amounts. Substitution of Mo^{6+} at the Zr or Si sites should shorten Zr-O distances and lengthen Si-O distances, consistent with our observations (Fig. 3). However, the concentrations of Mo measured by SIMS are insufficient to charge balance excess REE^{3+} in HREE-doped zircons by either of the above coupled substitutions alone, being approximately one half of the amount required (Hanchar et al. 2001).

Another effective way to provide charge balance in zircon crystals for which REE exceed P is by incorporating cations into interstitial sites. The zircon structure contains two interstitial sites that are potential sites for charge-balancing species, provided these sites can accommodate such elements without excessive strain. One interstitial site is a distorted octahedral site that shares two faces with two SiO_4 tetrahedra. The only additional elements available to synthetic zircon crystals in this study were Li and Mo from the flux. The proximity of two Si^{4+} ions (each at 1.84 Å) makes this an unlikely site for highly charged ions such as Mo^{6+}, Zr^{4+}, or REE^{3+}. This octahedral interstice lies approximately 1.87 Å from two O sites and 2.08 Å from four O sites. The ionic radius of six-coordinated Li^+ is 0.76 Å (Table 4), and the sum of effective ionic radii for four-coordinated O^{2-} (the coordination of O^{2-} bonded to an interstitial cation) and $^{VI}Li^+$ is 2.15 Å (Table 4), indicating that $^{VI}Li^+$ would be slightly over-bonded at this site. Nevertheless, minor Li^+ might be incorporated into this interstice.

In addition to the octahedral interstice, a four-coordinated interstitial site occurs adjacent to the octahedral interstice, sharing a face with it. This four-coordinated site lies within channels that run parallel to the *c* axis in the zircon structure (Fig. 5). The fractional coordinates for this distorted tetrahedral interstitial site are $x = 0.204$, $y = 0.5$, $z = 0$, and the site is 1.84 Å from the four adjacent O sites. The ionic radii of four-coordinated Li^+ and Zr^{4+} are both 0.59 Å, and the sum of effective ionic radii for $^{[IV]}O^{2-}$ (1.39 Å) and either $^{[IV]}Li^+$ or $^{[IV]}Zr^{4+}$ is 1.98 Å (Table 4); thus both cations would be slightly over-bonded at this site. The ionic radius of Mo^{6+} in four coordination is 0.41 Å, and the sum of effective ionic radii is 1.80 Å (Table 4). The four-coordinated interstitial site in $ZrSiO_4$ can therefore accommodate Mo^{6+} especially well, with little or no over-bonding and, we propose, relatively little strain.

Heavy REE^{3+} ions, with ionic radii of approximately 1.00 Å (Table 4), are clearly incapable of entering either interstitial site in quantities sufficient to account for "excess" REE in synthetic HREE-doped zircon crystals. Besides, if we could attribute all "excess" REE in HREE-doped zircon crystals (0.3–0.6 mol%) to interstitial REE, electron densities at interstitial sites should be measurable, whereas electron densities at interstitial sites are negligible in all synthetic zircon crystals with HREE and P. Furthermore, interstitial REE^{3+} would present a significant problem in terms of a likely charge-balance mechanism.

The incorporation of Li, Mo and, possibly, Zr into interstitial sites would maintain local charge neutrality where REE^{3+} replaces Zr^{4+} according to the substitutions,

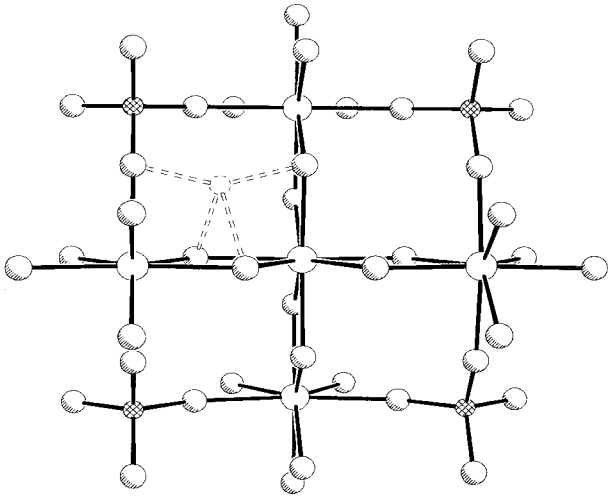

FIGURE 5. Zircon structure viewed approximately down [001] showing interstitial cavities and proposed four-coordinated interstitial site (dashed circle and dashed bonds). Large hollow circles represent Zr atoms; small cross-hatched circles represent Si atoms; highlighted circles represent O atoms.

$$Zr^{4+}_{(int)} + 4\ REE^{3+} = 4\ Zr^{4+}, \quad (1)$$

$$Li^{+}_{(int)} + REE^{3+} = Zr^{4+}, \quad (2)$$

and

$$Mo^{6+}_{(int)} + 6\ REE^{3+} = 6\ Zr^{4+}. \quad (3)$$

These substitutions are potentially important in HREE-doped synthetic zircon crystals, although interstitial Zr^{4+} and Mo^{6+} are most effective. A serious difficulty with proposing interstitial Zr^{4+} cations arises from the fact that Zr-site cations are negatively correlated with Si-site cations (Hanchar et al. 2001), strongly suggesting that excess Zr^{4+} occupies Si sites rather than interstitial sites. We cannot eliminate substitution 2 and 3, as Li and Mo are not present in quantities sufficient to be detected by XRD, especially considering that interstitial cations must be disordered. However, SIMS data demonstrate that Mo and Li correlate well with REE and P contents and that the apparent charge deficit (equal to P – REE) is strongly correlated with the molar content of Li plus six times the molar content of Mo (see Fig. 5 in Hanchar et al. 2001). Thus, combined structural and chemical data provide compelling evidence that Mo and Li occupy interstitial sites in synthetic zircon crystals for which HREE exceeds P.

We are left with an important question: what is the driving force that would lead to the incorporation of interstitial cations in the zircon structure? Surely, interstitial sites are unfavorable cation sites. The answer is that for small substitutions, P^{5+} imparts little local strain, but as concentrations of P and REE increase, strain at both Zr and Si sites increases. Increased strain at the Zr site, caused by substitution of large REE^{3+} cations, is mitigated somewhat because the ionic radii of REE decrease with increasing atomic number. No similar reduction of strain at the Si site is possible however, because, as REE concentrations increase, so too must P concentrations (and the ionic radius of P is fixed!).

Strain caused by increasing REE and P substitution at the Zr and Si sites is apparent in Figure 6. As REE concentrations increase, bond distances increase most sharply for the short Zr-O bond. The long Zr-O bond distance (Zr-O') increases more gradually and remains similar to the long Zr-O bond distance in $ZrSiO_4$ (2.130 Å). Notably, both Zr-O bond distances display maximum strain for the Er-doped crystal (crystal 36). Although greater amounts of HREE are incorporated at the Zr site, HREE are closer in size to Zr than light and middle REE, and therefore impart proportionately less strain for higher REE contents. Figure 6 also shows that the length of the Si-O bond decreases unabated as HREE concentrations increase. Thus, excessive strain at the Si site due to increased P substitution explains the inability of zircon crystals to incorporate sufficient P^{5+} to charge balance HREE, despite the increased compatibility of HREE in the zircon structure.

The inability of the Si site to incorporate sufficient P to charge balance REE^{3+} ions that are increasingly compatible in the zircon structure must be the primary reason that interstitial cations become incorporated into zircon. Of course, even small substitutions of, e.g., Mo^{6+} in an interstitial site should impart significant strain; however, the high charge of the Mo^{6+} ion makes it highly effective for charge balancing excess HREE. For zircon crystals synthesized in an anhydrous Li, Mo-oxide flux, no other charge-compensating cations are available, although other charge-balance mechanisms might operate in natural zircon crystals.

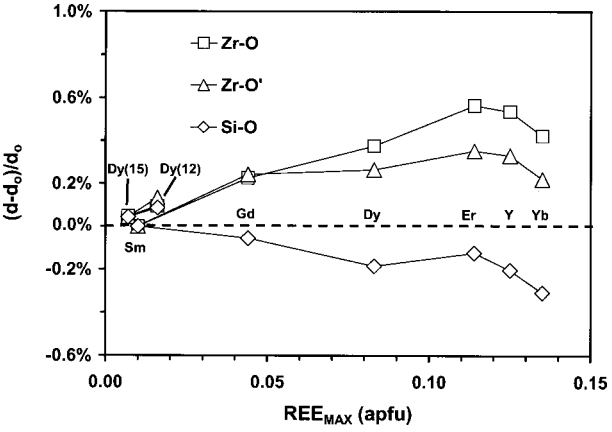

FIGURE 6. Structural strain as a function of increasing REE apfu in synthetic zircon crystals. Strain is expressed as the proportional change in cation-oxygen bond lengths relative to the equivalent bond distance (d_o) the [Sm+P]-doped crystal (crystal 28).

Clearly, limits on REE substitutions in these synthetic zircon crystals are not a simple function of REE^{3+} ionic radii but depend in a complex way on available charge-balance substitutions and structural strain associated with both Zr and Si sites. An important point to remember is that structural strain determined by XRD represents local strains averaged over whole crystals, from REE- and P-rich cores to crystal rims with much lower concentrations. Local strains within the central regions of zircon crystals, from which maximum REE and P concentrations were measured, must be quite high indeed. Maximum strains within crystal cores must be approximately 2/3 greater than (i.e., 166% of) the whole-crystal average strain as measured by XRD. This maximum strain determines the upper limits REE and P substitution in synthetic zircon crystals.

Because of charge-balance requirements for the coupled xenotime substitution, the exact mechanisms that determine the degree to which REE may substitute for Zr in natural zircons will depend on the geochemical environment in which crystals form. As noted in the Introduction, most natural systems contain additional elements that might contribute to charge compensation in zircon (Speer 1982), but all charge-balance mechanisms will induce some degree of structural strain in addition to that imposed by REE substitution at the Zr site. Blundy and Wood (1994) provided a straightforward model for predicting mineral-melt partition coefficients, based on strain induced by the element of interest; however, their model ignores ionic charge and the implications of coupled substitution. Our conclusion, that coupled REE and P substitution in synthetic zircon crystals is a function of strain at both cation sites involved, suggests that partition coefficients predicted by the Blundy and Wood model will be inaccurate unless all strain-inducing substitutions are considered.

Finally, it has been suggested that, whereas changing melt composition may change absolute REE concentrations in a

given mineral, REE do not fractionate differentially as a function of melt composition (Watson 1976; Ryerson and Hess 1978); that is, changing REE concentrations in a melt will change all REE in a mineral proportionately. Our results suggest that this is not quite true, because changing the availability of a charge-compensating element, such as P, can greatly enhance HREE substitution in zircon, whereas P substitution into zircon does not enhance LREE substitution. Although our results strictly apply only to zircon, we suspect that a similar conclusion pertains to all coupled substitutions in minerals where more than one structural site is involved.

ACKNOWLEDGMENTS

This research was supported in part by the National Science Foundation, grants EAR-8904177, EAR-9205793, EAR-9220095, and EAR-9527014 to E. B. Watson. The Environmental Management Sciences Program of the United States Department of Energy provided additional support for RJF and PCB (DE-FG07-97ER14820). X-ray diffraction data were collected at the Department of Civil Engineering and Geological Sciences, University of Notre Dame. We are grateful to D. Zhao and an anonymous reviewer for comments that helped clarify the paper.

REFERENCES CITED

Altermann, W. and Nelson, D.R. (1998) Sedimentation rates, basin analysis and regional correlations of three Neoarchean and Paleoproterozoic sub-basins of the Kaapvaal craton as inferred from precise U-Pb zircon ages from volcaniclastic sediments. Sedimentary Geology, 120, 225–256.

Azavant, P. and Lichanot, A. (1993) X-ray scattering factors of oxygen and sulfur ions: an *ab initio* Hartree-Fock Calculation. Acta Crystallographica, A49, 91–97.

Bea, F. (1996a) Residence of REE, Y, Th and U in granites and crustal protoliths; implications for the chemistry of crustal melts Granada, Spain. Journal of Petrology, 37, 521–552.

———(1996b) Controls on the trace element chemistry of crustal melts. Transactions of the Royal Society of Edinburgh: Earth Sciences, 87, 33–41.

Belousov, E.A., Griffin, W.L., and Pearson, N.J. (1998) Trace element composition and cathodoluminescence properties of southern African kimberlitic zircons. Mineralogical Magazine, 62, 355–366.

Blundy, J., and Wood, B. (1994) Prediction of crystal-melt partition coefficients from elastic moduli. Nature, 372, 452–454.

Bowring, S.A. (1995) The Earth's early evolution. Science, 269, 1535–1540.

Bowring, S.A., Erwin, D.H., Jin, Y.G., Martin, M.W., Davidek, K., and Wang, W. (1998) U/Pb zircon geochronology and tempo of the end-Permian mass extinction. Science, 280, 1039–1045.

Brown, I.D. (1981) The bond-valence method: An empirical approach to chemical structure and bonding. In M. O'Keefe and A. Navrotsky, Eds., Structure and Bonding in Minerals, vol. II, p. 1–30. Academic Press, New York.

Buick, R., Thornett, J.R., McNaughton, N.J., Smith, J.B., Barley, M.E., and Savage, M. (1995) Record of emergent continental crust similar to 3.5 billion years ago in the Pilbara craton of Australia. Nature, 375, 574–575.

Burns, P.C. (1998) CCD area detectors of X-rays applied to the analysis of mineral structures. Canadian Mineralogist, 36, 847–854.

Caruba, R., Baumer, A., Ohnenstetter, D., Cesbron, F., Rouer, O., and Blanc, P. (1995) The hydrothermal synthesis of molybdenum, sulfur-doped zircon: a study of charge compensation mechanisms. Neues Jahrbuch für Mineralogie-Monatshefte, 6, 241–254.

Chakoumakos, B.C., Murakami, T., Lumpkin, G.R., and Ewing, R.C. (1987) Alpha-decay–induced fracturing in zircon: The transition from the crystalline to the metamict state. Science, 236, 1493–1600.

Cherniak, D.J., Hanchar, J.M., and Watson, E.B. (1997) Diffusion of tetravalent cations in zircon. Contributions to Mineralogy and Petrology, 127, 383–390.

Crocombette, J.P. (1999) Theoretical study of point defects in crystalline zircon. Physics and Chemistry of Minerals, 27, 138–143.

Ellsworth, S., Navrotsky, A., and Ewing, R.C. (1994) Energetics of radiation damage in natural zircon ($ZrSiO_4$). Physics and Chemistry of Minerals, 21, 140–149.

Ewing, R.C. (1999) Nuclear waste forms for actinides. Proceedings of the National Academy of Sciences, 96, 3432–3439.

Ewing, R.C. and Lutze, W. (1997) Disposing of plutonium. Science, 275, 737.

Fujimaki, H. (1986) Partition coefficients of Hf, Zr, and REE between zircon, apatite, and liquid. Contributions to Mineralogy and Petrology, 94, 42–45.

Gibson, G.M. and Ireland, T.R. (1995) Granulite formation during continental extension in Fiordland, New Zealand. Nature, 375, 479–482.

Gromet, L.P. and Silver, L.T. (1983) Rare earth element distributions among minerals in a granodiorite and their petrogenetic implications. Geochimica et Cosmochimica Acta, 47, 925–939.

Hanchar, J.M., Miller, C.F., Wooden, J.L., Bennett, V.C., Staude, J.-M.G. (1994) Evidence from xenoliths for a dynamic lower crust, eastern Mojave desert, California. Journal of Petrology, 35, 1377–1415.

Hanchar, J.M., Finch, R.J., Hoskin, P.W.O., Watson, E.B., Cherniak, D.J., and Mariano, A.N. (2001) Rare earth elements in synthetic zircon: Part 1. Synthesis, and rare-earth element and phosphorous doping of zircon. American Mineralogist, 86, 667–680.

Hazen, R.M. and Finger, L.W. (1979) Crystal structure and compressibility of zircon at high pressure. American Mineralogist, 64, 196–201.

Heaman, L.M., Bowins, R., and Crocket, J. (1990) The chemical composition of igneous zircon suites: Implications for geochemical tracer studies. Geochimica et Cosmochimica Acta, 54, 1597–1607.

Hinton, R.W. and Upton, B.G.J. (1991) The chemistry of zircon: Variations within and between large crystals from syenite and alkali basalt xenoliths. Geochimica et Cosmochimica Acta, 55, 3287–3302.

Ibers, J.A. and Hamilton, W.C., Editors. (1974) International Tables for X-ray Crystallography, vol. IV. The Kynoch Press, Birmingham, U.K.

King, E.M., Barrie, C.T., and Valley, J.W. (1998) Hydrothermal alteration of oxygen isotope ratios in quartz phenocrysts, Kidd Creek mine, Ontario: Magmatic values preserved in zircons—Reply. Geology, 26, 764.

Lee, J.K.W., Williams, I.S., and Ellis, D.J. (1997) Pb, U and Th diffusion in natural zircon. Nature, 390, 159–162.

Maas, R., Kinny, P.D., Williams, I.S., Froude, D.O., and Compston, W. (1992) The Earth's oldest known crust; a geochronological and geochemical study of 3900-4200 Ma old detrital zircons from Mt. Narryer and Jack Hills, Western Australia. Geochimica et Cosmochimica Acta, 56, 1281–1300.

McLaren, A.C., Fitz Gerald, J.D., and Williams, I.S. (1994) The microstructure of zircon and its influence on the age determination from Pb/U isotopic ratios measured by ion microprobe. Geochimica et Cosmochimica Acta, 58, 993–1005.

Meldrum, A., Zinkle, S.J., Boatner, L.A., and Ewing, R.C. (1998) A transient liquid-like phase in the displacement cascades of zircon, hafnon and thorite. Nature, 395, 56–58.

Murakami, T., Chakoumakos, B.C., Ewing, R.C., Lumpkin, G.R., and Weber, W.J. (1991) Alpha-decay event damage in zircon. American Mineralogist, 76, 1510–1532.

Nagasawa, H. (1970) Rare earth concentrations in zircons and apatites and their host dacites and granites. Earth and Planetary Science Letters, 9, 359–364.

Odling, N.W.A. (1995) An experimental replication of upper-mantle metasomatism. Nature, 373, 58–60.

Riggs, N.R., Lehman, T.M., Gehrels, G.E., and Dickinson, W.R. (1996) Detridal zircon link between headwaters and terminus of the Upper Triassic Chinle-Dockum paleoriver system. Science, 273, 97–100.

Rollinson, H.R. (1993) Using geochemical data: evaluation, presentation, interpretation. Longman Scientific and Technical, New York.

Ryerson, F.J. and Hess, P.C. (1978) Implications of liquid-liquid distribution coefficients to mineral-liquid partitioning. Geochimica et Cosmochimica Acta, 42, 921–932.

Shannon, R.D. (1976) Revised effective ionic radii and systematic studies of interatomic distances in halides and chalcogenides. Acta Crystallographica, A32, 751–767.

Solar, G.S., Pressley, R.A., Brown, M., and Tucker, R.D. (1998) Granite ascent in convergent orogenic belts: Testing a model. Geology, 26, 711–714.

Speer, J.A. (1982) Zircon. In P.H. Ribbe, Ed., Orthosilicates, vol. 5, p. 67–112. Reviews in Mineralogy, Mineralogical Society of America, Washington, D.C.

Stein, H.J., Sundblad, K., Markey, R.J., Morgan, J.W., and Motuzuma, G. (1998) Re-Os ages for Archean molybdenite and pyrite, Kuittila-Kivisuo, Finland, and Proterozoic molybdenite, Kabeliai, Lithuania: Testing the chronometer in a metamorphic and metasomatic setting. Mineralium Deposita, 33, 329–345.

Taylor, B.E. and Huston, D.L. (1998) Hydrothermal alteration of oxygen isotope ratios in quartz phenocrysts, Kidd Creek mine, Ontario: Magmatic values preserved in zircons. Geology, 26, 763–764.

Vervoot, J.D., Patchett, P.J., Gehrels, G.E., and Nutman, A.P. (1996) Constraints on early Earth differentiation from hafnium and neodymium isotopes. Nature, 379, 624–627.

Watson, E.B. (1980) Some experimentally determined zircon/liquid partition coefficients for the rare earth elements. Geochimica et Cosmochimica Acta, 44, 895–897.

Watson, E.B., Cherniak, D.J. Hanchar, J.M., Harrison, T.M., and Wark, D.A. (1997) The incorporation of Pb into zircon. Chemical Geology, 141, 19–31.

Williford, R.E., Weber, W.J. Devanathan, R., and Cormak, A.N. (1999) Native vacancy migrations in zircon. Journal of Nuclear Materials, 273, 164–170.

MANUSCRIPT RECEIVED MAY 27, 1999
MANUSCRIPT ACCEPTED JANUARY 18, 2001
MANUSCRIPT HANDLED BY RODNEY C. EWING